J Mater Sci (2011) 46:7611–7619
DOI 10.1007/s10853-011-5738-7

Effect of salt composition on photovoltaic performance of the dye-sensitized solar cells prepared from nano anatase TiO_2 powder using NaCl–$Na_2HPO_4{\cdot}2H_2O$ salt matrices

B. Roy · L. Li · S. Aich

Received: 16 April 2011 / Accepted: 21 June 2011 / Published online: 8 July 2011

Abstract Photovoltaic performances of dye-sensitized solar cells based on mesoporous TiO_2 coating of nanocrystalline anatase prepared by solid salt synthesis were investigated in this study. Three different salt compositions pure NaCl, NaCl and DSP 50–50 wt% mixture, and pure DSP have been used as the reaction mediums. The best photovoltaic performances were obtained for the device made using the powder from DSP matrix. The dye-sensitized solar cells built from DSP and NaCl50 powders showed 13.8 and 6.5% improvements in the short-circuit current density, and 34 and 20% improvement in overall efficiency, respectively, than those of the cell made from Degussa P-25 powder. These results have been explained from the microstructural point of view of the powders. Electron microscopy, XRD, Raman, and nitrogen adsorption–desorption studies showed that the coatings made from the powders obtained via NaCl 50 and DSP salt medium treatments were of smaller sizes and contained higher densities of narrower mesoporous distribution than that obtained by the coating from NaCl and no-salt-synthesized materials.

B. Roy (✉)
Department of Materials Engineering, New Mexico Institute of Technology, Socorro, NM 87801, USA
e-mail: broy@nmt.edu

L. Li
PRRC, New Mexico Institute of Technology, Socorro, NM 87801, USA

S. Aich
Department of Metallurgical and Materials Engineering, Indian Institute of Technology, Kharagpur 721302, India

Introduction

Photo-electrochemical effect of the dye-sensitized solar cell (DSSC) is a combination of multiple steps, and hence proper tuning is essential in every step to achieve high energy conversion. DSSCs are based on the high surface area of mesoporous semiconductor anode (such as; TiO_2, ZnO, and Nb_2O_5) [1], and effective charge transfer through the interconnected nanocrystals. Therefore, the method of preparation for the anode is very important. Several studies have been published on the preparation of DSSCs from nano TiO_2 powders made by low-temperature sol–gel, hydrothermal, and other solution chemical routes [2–5]. Adachi et al. synthesized single crystal-like anatase TiO_2 nanowires formed in a network structure by surfactant-assisted self-assembling processes at low temperature and built solar cell of high efficiency [2]. Barbe et al. reported high efficacy of solar cell built on the mesoporous and nanostructured films of nano anatase powder grown under the mixed sol–gel and hydrothermal technique at low temperature [3]. Fujimoto et al., fabricated DSSCs simultaneously by an electrospray and conventional coating methods using TiO_2 nanocrystal dispersion of commercially available P-25 in water and compared their photovoltaic characteristics [4]. Jiu et al. reported preparation of low temperature nanocrystalline anatase powder, based on a mixed template of a copolymer and a surfactant, and used this powder to build DSSCs [5]. The nanocrystals grown at lower temperatures may contain high density of defect states. Particles with higher defects may increase the speed of the electron transfer from dye to TiO_2 as the defects states are located below the conduction band of the semiconductor, but these defect states may trap the electrons and decrease the total charge transfer, and the overall efficiency suffers as a consequence [6]. TiO_2 particles of

higher crystallinity can facilitate the process of electron injection from dye to TiO_2 and further transport toward the TCO, although high crystallinity may need high treatment temperature; on the other hand, sintered particles can increase the size and decrease surface area.

We have demonstrated that the use of salt matrices in solid state can control particle size of anatase TiO_2 powder [7, 8]. Microstructural exploration of two groups of anatase and rutile samples showed that, even up to relatively high-temperature treatments (but salt still remains in completely solid state), sintering of the powder is limited and nano-crystalline particles are possible to achieve. When we tried three different salt compositions as the reaction medium; pure NaCl, NaCl and DSP 50–50 mixture, and pure DSP, the smallest particle growth was observed for the pure DSP samples. In this article, we present a preliminary study on photovoltaic characterization of DSSCs based on the TiO_2 powders prepared using salt matrices and compare these properties with those of the commercially available Degussa P-25 powder.

Experimental procedure

Powder preparation

Amorphous titanium hydroxide, sodium chloride (Aldrich, >99%), and dibasic sodium hydrogen phosphate ($Na_2HPO_4{\cdot}2H_2O$, Fisher, >99%) (DSP) were used as the starting materials. Titanium hydroxide was precipitated from Ti(IV)-chloride (Alfa Aesar, >97%, $TiCl_4$), by hydrolysis with aqueous ammonia (NH_3:H_2O = 1:1 molar ratio). The gelatinous and amorphous precipitate was washed with distilled water several times until it became NH_3 or Cl^- free. A mixture of precipitate (as TiO_2) and salt in the weight ratio of 4:5 was ball milled in deionized (DI) water. NaCl and DSP either as a single component or as a mixture by weight percentage (wt%) as 100:0 (hereafter called as NaCl sample), 50:50 (hereafter called as NaCl50 sample), and 0:100 (hereafter called as DSP sample) were used for the salt matrix. The mixed slurry was dried at room temperature under a fume hood and then lightly ground into powder with mortar and pestle. For heat treatment, the powder was placed in a closed alumina crucible and placed inside the furnace at a pre-set temperature. The powders were heated at 725 °C for 3 h to achieve pure anatase phase and then quenched into DI water. The quenched mass was washed with hot 0.1 M HCl followed by DI water several times and centrifuged to eliminate the extra sodium, chlorine, and phosphorous salts. The mass was dried at ~100 °C and collected as powder. Samples were found to be slightly yellowish in color. An undoped or no-salt sample was heat treated simultaneously, and this no-salt powder and a commercially available Degussa P-25 TiO_2 powder were characterized side by side for the comparison basis.

Preparation of titania coating and solar cells

The indium–tin–oxide (ITO)-coated (15–18 Ω/sq, SPI supplies, 80% transparent, and 250 nm thick) glass slides (1 cm × 1 cm, 1.1 mm thick) were used as the substrate for the preparation of TiO_2 coating. The conducting glass substrates were cleaned using water solution of 10 wt% alkonox by ultrasonication twice, with DI water by ultrasonication twice, using acetone and ultrasonic twice, and finally by oxygen plasma. These substrates were dried in air. Titania pest was prepared by mixing 10 g of TiO_2 powder in a mortar with 2 cc of ethylene glycol and 12 cc nitric acid–water solutions (pH 3–4). These pastes were applied repetitively to the conducting glass (ITO) as follows.

An adhesive tape was utilized to secure these clean and air-dry substrates on a flat plate, to control the thickness of the coating as well, and to provide a bare electrode used as contact during electrical characterization. The titania pastes were applied at one free edge of the substrate and spread evenly along the surface with a glass rod. For the thicker samples, coating was applied multiple times. After each coating, the sample was dried slowly at room temperature in a homemade humidity-controlled box and calcined at 450 °C for 30 min after drying. Finally, after last coating, the sample was calcined at 450 °C for 60 min. These films were immersed in an ethanol solution (2×10^{-4} M) of cis–bis (isothiocyanato) bis (2, 2′-bipyridyl-4, 4′-dicarboxylato)-ruthenium (II) (N3) dye for overnight at 50 °C for adsorption. Next day, these impregnated electrodes were rinsed carefully in absolute ethanol and air dried. Another cleaned ITO-coated glass substrate, with ~50-nm-thick carbon catalyst layer (deposited by evaporation, EMITECH K9550) and heat treated at 450 °C for 15 m, was used as the counter electrode. The TiO_2 electrode and the counter electrode were placed carefully face to face (slightly offset to accommodate electrode contact to alligator clips for electrical measurement) with a 30-μm-thick spacer in between them and secure by paper holding clips to assemble the DSSCs. The electrolyte (KI/KI_3 redox couple) was made by mixing 0.5 M KI in 10 cc dry ethylene glycol and 0.05 M KI_3 in 10 cc dry ethylene glycol together. A drop of this solution was introduced into the cell by capillary force just before the measurement.

Characterization

X-ray diffraction (Siemens D 500 system with a CuK_α radiation, operated at 40 kV and 30 mA) of all the prepared

samples was performed over a 2θ range of 20–70° to determine the phase content. The grain sizes (d_{XRD}) were calculated from the full-width at half-maxima (FWHM) of 100% anatase (101) by Scherrer's formula [9]. Surface areas of the samples were measured using a Micromeritics ASAP 2020 nitrogen absorption/desorption porosimeter (Norcross, GA) and the single-point Brunauer–Emmett–Teller (BET) method, using the adsorption data in the relative pressure ($P/P0$) range of 7.8×10^{-6}–0.99, and desorption from 0.99 to 0.14. The particle size distribution was calculated from the desorption isotherms and the Barrett–Joyner–Halender (BJH) method, with cylindrical pore size being calculated from the Kelvin equation that was used in data processing. Microstructures of the powders were studied with a field emission scanning electron microscope (FESEM, Hitachi S-800) at 15 kV. Powder samples were coated with 5–10 nm gold coating for better conductivity to minimize charging of the sample. A transmission electron microscope (TEM, Hitachi H-7000 FA) was also used for microstructural characterization of the powders. The TEM specimens were prepared from the suspension of powder in ethanol and a LaB_6 filament at 125 kV was used as the electron beam source. A LabRAM ARAMIS integrated confocal micro Raman system from HORIBA Jobin–Yvon equipped with 632.8 nm He–Ne laser as the excitation light source was used to examine the samples. The unpolarized scattered light was collected for 1-s acquisition time in the backscattering geometry using a multichannel CCD detector. The incident laser power was 50 mW for the measurements in air. The spectrometer was calibrated using Raman active Γ_{25} phonon peak of diamond-structured single crystal Si wafer at ~ 520 cm^{-1}. A resolution of 1 cm^{-1} for the Raman peak position and peak width (full width at half maximum—FWHM) was obtained.

The photovoltaic properties for the fabricated cells were measured using a solar simulator (Sciencetech model SS, 1.6 kW) under irradiation of a xenon short arc lamp using AM 1.5 filtering condition with light intensity of 1 sun (100 mW/cm^2) and a Keithley source meter 2400. The effective cell size was 0.25 cm^2.

Results and discussion

Photovoltaic performances of the solar cells made from the coatings of different powders and thicknesses were measured. Figure 1 depicts the best *I–V* results obtained for the anode coatings. Variations of the nature of the curves and short circuit current (I_{sc}) depending on different salt systems are noticeable, but open circuit voltage (V_{oc}) values do not change much. The highest I_{sc}, V_{oc}, energy conversion efficiency (η), and fill factor (FF) were measured to be 14 mA/cm^2, 0.67 V, 6.3, and 67.5%, respectively for the DSP sample of thickness 7.6 μm. The second best performance was claimed by the NaCl50 sample with I_{sc}, V_{oc}, η, and FF values of 13.1 mA/cm^2, 0.66 V, 6, and 65.5%, respectively for a 8.1-μm-thick coating anode. The V_{oc} value of the device made from P-25 powder was same as

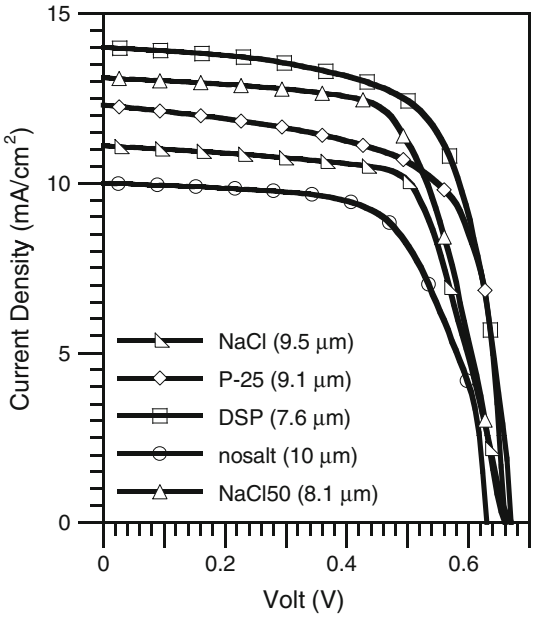

Fig. 1 The best *I–V* responses of the devices prepared from the coatings of different powders

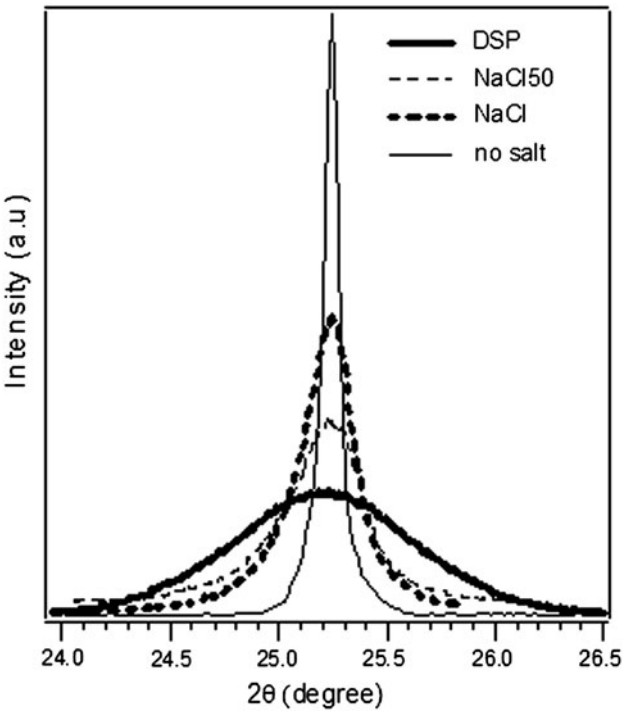

Fig. 2 The anatase (101) XRD peak from the powders treated with different salt compositions. Variation of FWHM with different salt treatments is clearly seen

that of the DSP powder, although I_{sc}, η, and FF values were 22.8, 34, and 6%, respectively, lower than those of the DSP sample. The I_{sc}, V_{oc}, η, and FF values for the P-25 cell of thickness ~9.1 μm are close to the values (I_{sc} ~ 12 mA/cm^2, V_{oc} ~ 0.645 V, η ~ 5%, and FF ~ 63%) reported by Tan et al. [10] for their cell made from P-25 TiO_2, but the I_{sc} value is 25% higher than that (~9 mA/cm^2) measured by Adachi et al. for the similar kind of thickness of P-25 TiO_2 anode coating [2]. The variations of the *I–V* characteristics of the samples can be explained from the microstructure of the powders.

XRD analysis (Fig. 2) revealed that all the powders are randomly oriented single-phase anatase (indexed to tetragonal space group *I*41/*amd*). The FWHMs of the peaks vary significantly with the type of the treatment salt medium. For the DSP sample, FWHM of the anatase (101) XRD peak was measured to be ~0.9°, corresponding to the calculated average particle size ~9 nm, and, for the no-salt sample, the FWHM measured was found to be around the instrumental broadening (0.1°) value, pushing the particle size beyond the limit one could measure by general XRD: ≤100 nm [9].

Figure 3 shows the FESEM images of the coatings made from the powders of (a) DSP, (b) NaCl50, (c) NaCl, and (d) no-salt. The smallest and the largest particles (d_{SEM}) were obtained: in the range from 5 to 15 nm and from 80 to 120 nm for DSP and no-salt samples, respectively, consistent with the results previously reported [7, 8].

Figure 4 shows bright-field TEM images of the powders scraped out from the films. The sample from NaCl (Fig. 4b) is observed to be nanocrystallites of varying sizes (d_{TEM}) in the 15–50 nm range. For the powder from DSP (Fig. 4c), the particle size appears to be smaller with narrower distribution: 5–15 nm. In general, the particles were observed to be interconnected. The dashed circles in Fig. 4b and c shows the neck formation between particles clearly. The inset of Fig. 4c—HRTEM image of a particle of DSP powder—shows the defect-free lattice planes as an indication of the highly crystalline nature of the particles. The interplanar distance of the lattice fringes was measured

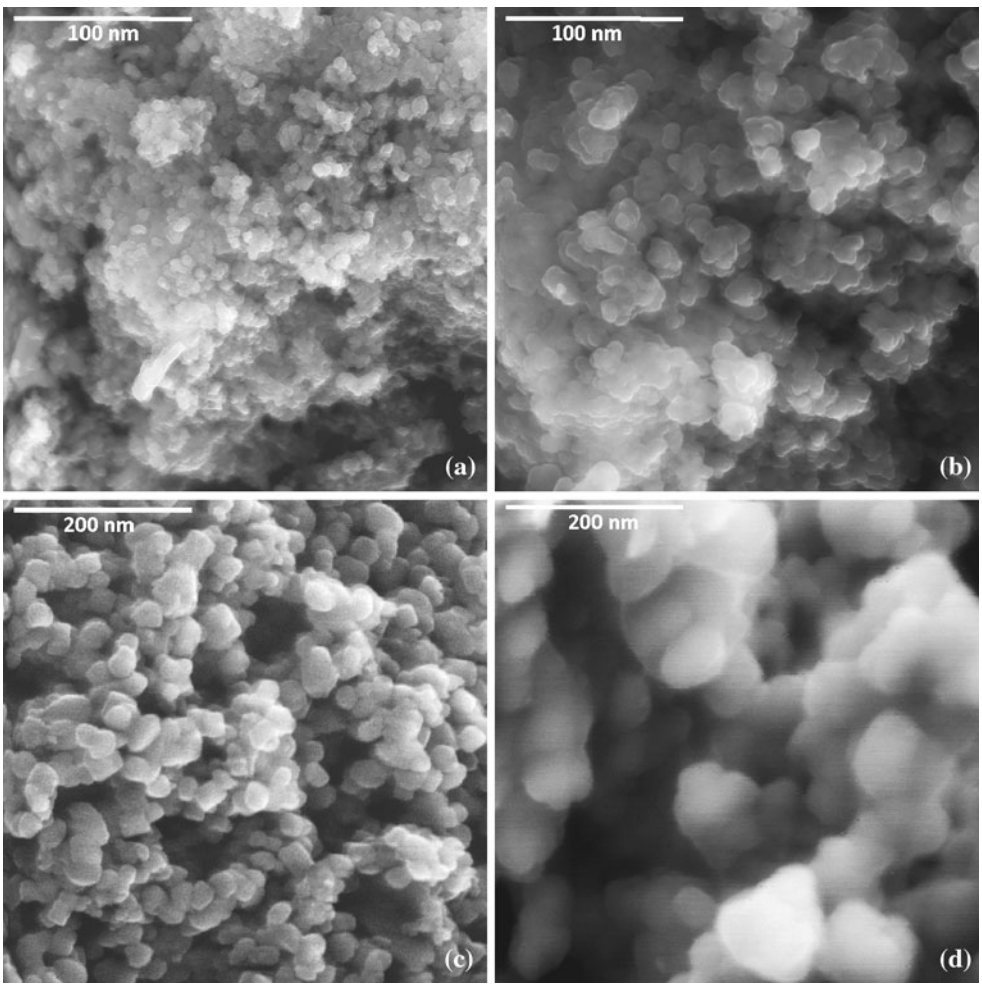

Fig. 3 FESEM images of the films prepared from the powders obtained with (**a**) DSP, (**b**) NaCl50, (**c**) NaCl, and (**d**) no-salt show the effect of the salt matrices on the microstructure of the powders

to be ~3.5 Å, which corresponds to that of anatase (101) planes. The selected area diffraction pattern rings (Fig. 4c) were indexed as single-phase anatase (101), (200), (004), (105), (204) planes indicating the random polycrystalline nature of the samples, these values being in agreement with the XRD results [7, 8]. The necking or contact areas between the particles and size of the particles as observed in powders did not change much after film preparation heat treatment procedure. On the contrary, Nakade et al. observed significant neck growth in the hydrothermally grown nano anatase TiO_2 powders during the film preparation procedure similar to the one adopted in this study [11]. This difference could be attributed to the fact that the salt-treated powders were already heated at a temperature much higher than that had been used for the film preparation, whereas the hydrothermally grown samples were made at lower temperature; 220 °C.

Figure 5a–d shows the nitrogen adsorption–desorption isotherms comparing the pore texture of the coatings, and the inset images show the pore size distribution for the corresponding samples. Figure 5a, b shows the isotherms for the DSP and NaCl50 powders mostly type IV with only one hysteresis loop of type H3 extended from P/P_0 range of 0.99 to 0.4—associated with aggregates of platelike particles, resulting in slitlike mesopores of monomodal distribution. Pore size distribution for the samples confirms this phenomenon. For the DSP sample, pore sizes are distributed within the range of 2–100 nm, but most of them are within mesoporous range (2–50 nm). For NaCl50 powder, this range is 10–30 nm. The isotherms for NaCl and no-salt

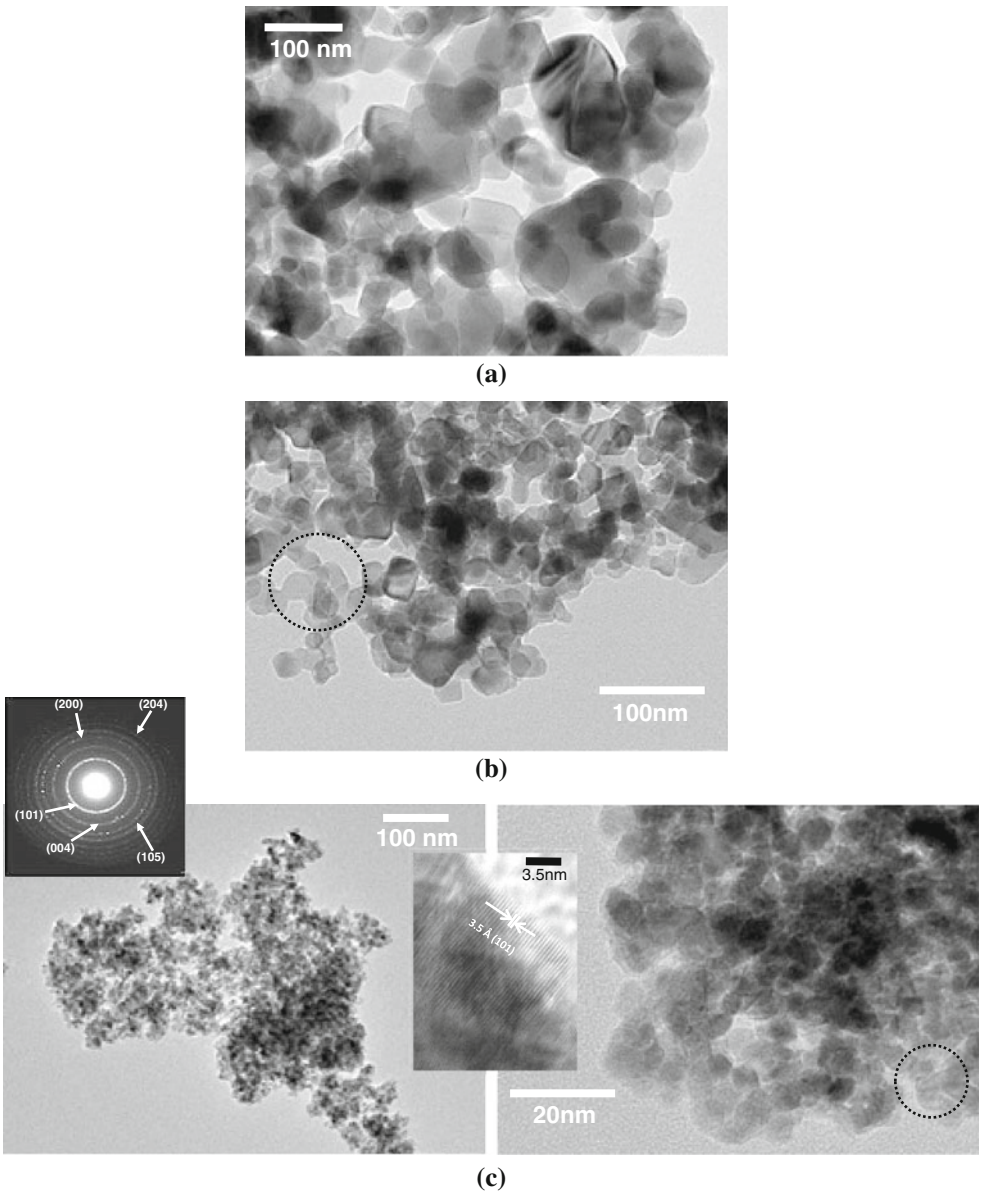

Fig. 4 Bright field TEM images of the powders prepared with (**a**) no-salt, (**b**) NaCl, and (**c**) DSP. The *dashed circles* in (**b**) and (**c**) show the neck formation between the particles. The *inset* of (**c**) shows the lattice fringes of the sample DSP. The inter lattice distance of ~3.5 Å corresponds to the interplanar distance of anatase (101) planes. The selected area diffraction pattern rings are indexed as single-phase anatase; (101), (004), (105), (200), and (204) planes indicate the random polycrystalline nature of the samples

powders are combination of type II and IV according to a classification proposed by IUPAC [12–15] and contain two hysteresis loops indicating bimodal distribution of pores. The hysteresis loop in the higher P/P_0 range is type H3 consists of larger, interparticle pores, while the hysteresis loops observed at lower P/P_0 range are H2 type—typical for the fine, intraparticle pores with narrow necks and wider bodies (ink-bottle pores) [16]. For the no-salt samples majority of the pores are in the macro pore region (50–100 nm). BET particle size (d_{BET}) was calculated from the measured surface area (S_{BET}) and theoretical density ($\rho = 3.9$ gm/cc) of anatase TiO_2 according to the relation $d_{BET} = 6/(\rho S_{BET})$, here it has been assumed that the particles are monodispersed and spherical [17, 18]. Average particle sizes calculated from XRD and BET, and measured from FESEM and TEM images are in good agreement. Table 1 summarizes the particle size and pore volume of all salt-synthesized TiO_2 powders. Data collected (manually and with the aid of Digital Micrograph 3.4, Gatan Inc, Pleasanton, CA) from the SEM and TEM images of at least 500 particles per sample were used for this statistical comparison.

Figure 6 shows the variations in the Raman spectra of the powders treated with different salt systems. In general, for an anatase sample within certain size limits (≤15 nm), the particle size reduction is proportional to the asymmetric peak broadening and blue shifting of the $E_{g(1)}$ mode at ~144 cm^{-1}, which has been chosen in view of its highest intensity among all the modes [19]. For the DSP sample, significant blue shift from 144 to 153 cm^{-1} and maximum

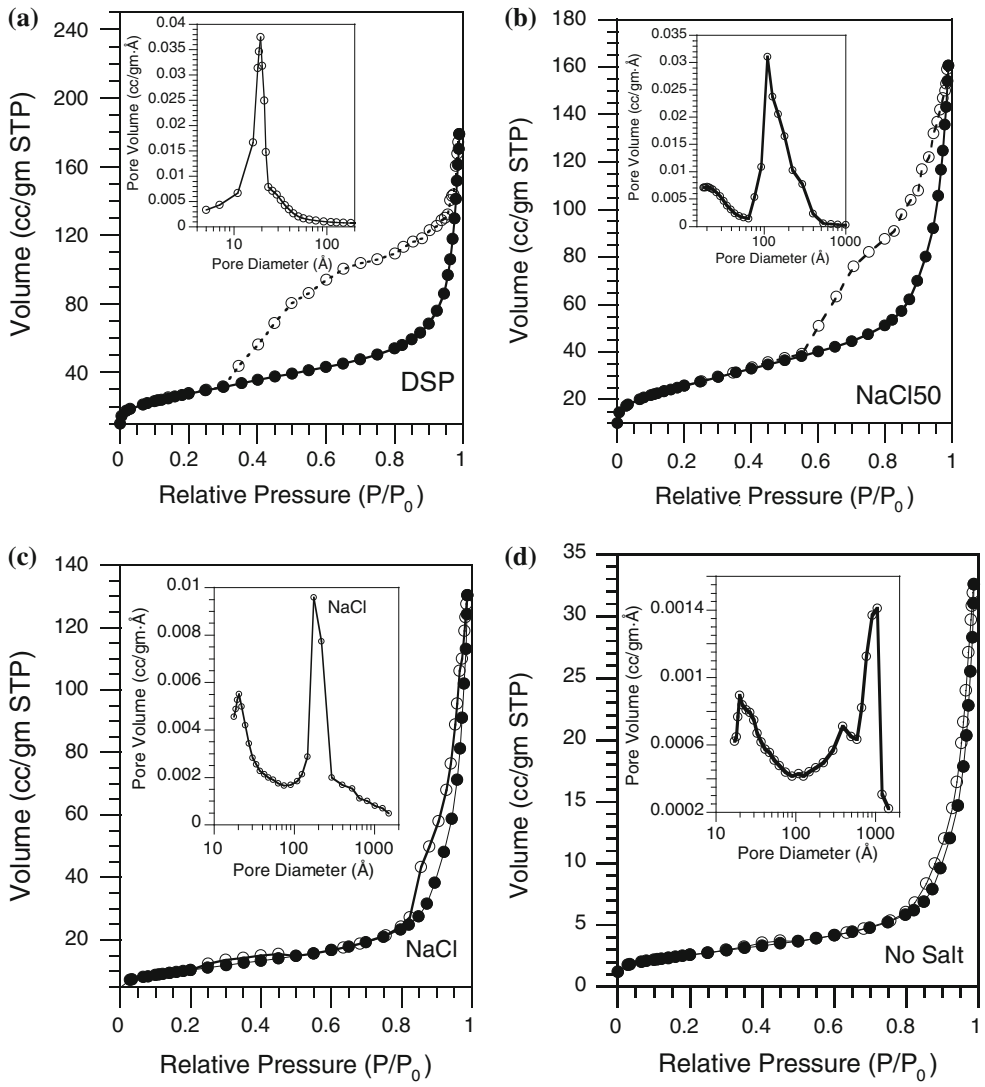

Fig. 5 Nitrogen adsorption (*solid circle*) and desorption (*hollow circle*) isotherms of the powders prepared with (**a**) DSP, (**b**) NaCl 50, (**c**) NaCl, and (**d**) no-salt. Isotherms of DSP and NaCl 50 are type IV, with one hysteresis loop corresponding to monomodal pore size distribution, while isotherms of NaCl and no-salt samples are combination of type II and IV, with two hysteresis loops corresponding to bimodal pore size distribution, as confirmed by the pore size distribution shown in the *inset*

Table 1 Particle size and pore volume of salt-synthesized TiO_2 powders

Sample	S_{BET} (m^2/g)	d_{BET} (nm)	d_{XRD} (nm)	d_{SEM} (nm)	d_{TEM} (nm)	Pore volume (cm^3/g)
DSP	100	16	9	5–15	5–15	0.26
NaCl50	90	18	23	10–30	10–30	0.21
NaCl	38	40	32	25–50	25–50	0.085
No-salt	13.4	115	≥100	80–120	80–120	0.02

peak broadening (20 cm^{-1}) of the $E_{g(1)}$ mode, and some blue shift for the $E_{g(2)}$ peak from ~200 to 236 cm^{-1} were obtained. The $B_{1g(1)}$ and $A_{1g} + B_{1g(2)}$ modes showed no shift, although significant peak broadenings of 45 and 42 cm^{-1}, respectively, occurred. The $E_{1g(3)}$ peak showed small blue shifting to 645 cm^{-1} with 36 cm^{-1} FWHM. As particle size increases, the $E_{g(1)}$ mode shows systematic red shifting to 141 cm^{-1} for no-salt and NaCl powders, and peak widths narrow down to ~10 cm^{-1}. The $E_{g(2)}$ mode (196 cm^{-1}) shows no shift, while $B_{1g(1)}$ mode at 395 cm^{-1} shows negligible red shift from 400 cm^{-1} with minimum

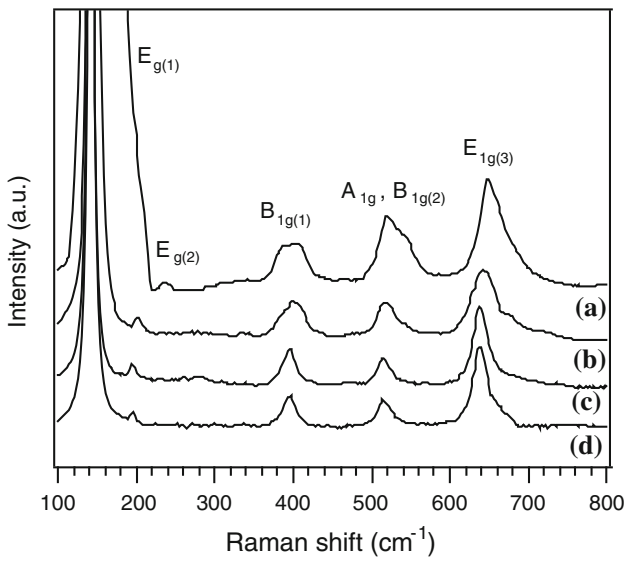

Fig. 6 Raman spectra of the powders with (**a**) DSP, (**b**) NaCl50, (**c**) NaCl, and (**d**) no-salt

FWHM (22 cm^{-1}) for both the samples. The $A_{1g} + B_{1g(2)}$ and $E_{g(3)}$ peaks show no shifting with almost the same FWHM (23 cm^{-1}). Powder from NaCl50 exhibits intermediate effects in terms of peak position and symmetry. Raman spectra of the samples are consistent with the microstructural and XRD analysis and confirm the pure anatase phase of the powders. Table 2 summarizes the Raman characteristics of the all salt-synthesized TiO_2 powders.

In previous study, it was found out that salt matrices retarded the particle growth. Depending on the salt matrix used, Cl^- and/or PO_4^{-3}/HPO_4^{-2} may be strongly bonded to the titanium hydroxide and/or TiO_2 surface, obstructing the necessary bond breakage, structural rearrangement, and mass transfer for growth [20–22]. In addition the salt envelop covering the particles acts as a physical diffusion barrier limiting the growth and minimizing the degree of aggregation of particles even up to relatively high temperature (725 °C). Because of imperfect dispersion and/or sublimation of some salt during heating, particle–particle contact may occur in some places and growth of the anatase may happen via normal solid-state mechanisms. For DSP, this effect is the most severe because the bigger size of the anion and mixed salts affects the microstructure of the powder and solar cell properties intermediately. The higher surface area may help higher amount of dye adsorption on the surface, increase electron recombination lifetime, and hence the best photovoltaic performance could be observed for the DSP sample [23]. In addition, smaller particles can increase the effective light absorption coefficients, and as a consequence, increase the amount of photogenerated electrons close to TCO. However, small particle size may contain higher density of surface and bulk defects, decrease carrier diffusion length (lower diffusion coefficient), and dye to TiO_2 charge injection efficiency [6]. The number of particles per unit area is higher for the smaller particles coatings too. Combination of these could be the possible cause for the saturation of the *I–V* characteristics at lower thickness for the DSP and NaCl50 coatings.

The better photoelectric performance of the DSP and NaCl50 powders over P-25 can be attributed mostly to smaller particle sizes and better inter-particle contact. Degussa P-25 is a widely investigated material. Hidalgo et al.

Table 2 Raman spectra characteristics of the salt-synthesized TiO_2 powders

Sample	$E_{g(1)}$		$E_{g(2)}$ Position (cm^{-1})	$B_{1g(1)}$		$A_{1g} + B_{1g(2)}$		$E_{g(3)}$	
	Position (cm^{-1})	FWHM (cm^{-1})		Position (cm^{-1})	FWHM (cm^{-1})	Position (cm^{-1})	FWHM (cm^{-1})	Position (cm^{-1})	FWHM (cm^{-1})
DSP	153	20	236	400	45	520	42	645	36
NaCl50	145	11	201	400	36	518	30	642	35
NaCl	141	10	196	395	22	517	22	638	23
No-salt	141	10	196	395	22	517	21	640	23

reported that the pore distribution of this powder covers a whole range of 2–50 nm with the average maximum at ~35 nm [24]. TEM study showed that Degussa P-25 TiO_2 is made of single crystalline anatase (~25 nm) and rutile (~85 nm) particles mixed in a ratio of about 3:1, where the anatase and rutile particles exist separately and charge transfer depends on the particle–particle mechanical contact via agglomeration [25, 26]. For DSP and NaCl50 powders, high crystallinity, smaller particle size, narrower mesoporous networking, and better necking between particles increase I_{sc} because of higher inner- and interparticle electron diffusion length, better charge transform from one particle to another, and higher recombination life time [11, 23]. For the NaCl and the no-salt powders, probably the lower surface area scales down these qualities.

Increasing thickness decreases the V_{oc} and FF both, but mixed results are observed for I_{sc} and η. As can be seen in Fig. 7b and d, for the DSP cell, as an example, V_{oc} and FF values decreased from 0.72 V and 69% to 0.58 V and 65% for 2.1 and 11.2 μm coatings, respectively. The I_{sc} and η values (Fig. 7a, c) initially increase from 5.1 mA/cm^2 and 2.5% for 2.1 to 14 mA/cm^2 and 6.3% for 7.6 μm coating and then decrease as the thickness increases. The η values for the P-25-based DSSCs of different thicknesses were noticed to be very consistent with the results reported by the others [10]. The decrease of V_{oc} and FF values with thickness can be attributed to the increase of the series resistance component of the cell circuit, increase of the electron–hole charge recombination centers, and attenuation of the available solar spectrum power density [27–29]. The I_{sc} values initially increase, which is probably due to increase of the adsorbed dye amount as a consequence of the increased surface area, but after crossing the optimum thickness threshold, increase of the recombination centers diminish the ultimate carrier collection [27].

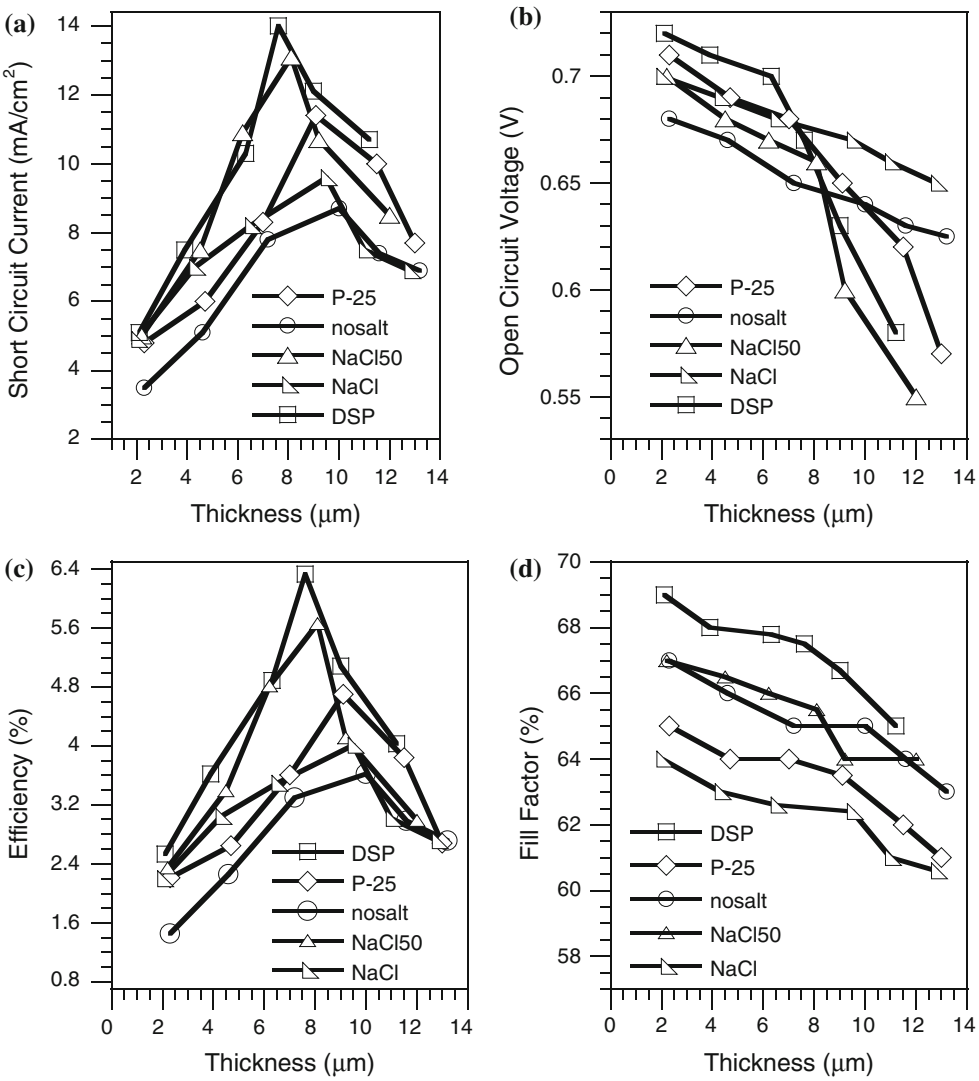

Fig. 7 Photovoltaic performances of the DSSCs built from the powders; variation of the (**a**) short circuit current (I_{sc}), (**b**) open circuit voltage (V_{oc}), (**c**) overall efficiency (η), and (**d**) fill factor (FF), respectively, depending on the coating thickness. All these devices were characterized under 1 sun (100 mW/cm^2) and AM 1.5 illumination

Conclusions

Nanocrystalline (≤20 nm) mesoporous anatase TiO_2 powder with high surface area, high crystallinity, and good inner particle contact through necking and can be made by using salt matrices of high melting point. Microstructural studies and the BET tests indicated that the anodic coatings prepared from NaCl 50 and DSP powders have smaller particle size and higher density of narrower pores than the NaCl and no-salt powders. As a consequence, DSSCs prepared from NaCl 50 and DSP powders demonstrated better photovoltaic performance than those prepared from NaCl and no-salt powders. For the solar cell built on the coating of TiO_2 powder prepared from DSP salt treatment at 725 °C for 3 h, the overall photon-to-current conversion efficiency was observed to increase by 34% higher than that of the commercially available Degussa P-25 powder, while for the no-salt samples obtained under same conditions, the conversion efficiency has been found to be 23% lower than that of the P-25. This result can be attributed to the better intraparticle contact and smaller particle size distribution of DSC sample than those of P-25.

References

1. Gratzel M (2000) Prog Photovolt Res Appl 8:171
2. Adachi M, Murata Y, Takao J, Jiu J, Sakamoto M, Wang F (2004) J Am Chem Soc 126:14943
3. Barbe CJ, Arendse F, Comte P, Jirousek M, Lenzmann F, Shklover V, Gratzel M (1997) J Am Ceram Soc 80:3157
4. Fujimoto M, Kado T, Takashima W, Kaneto K, Hayase S (2006) J Electrochem Soc 153:A826
5. Jiu J, Wang F, Sakamoto M, Takao J, Adachi M (2004) J Electrochem Soc 151:A1653
6. Benko G, Skarman BN, Wallenberg R, Hagfeldt A, Sundstrom V, Yartsev AP (2003) J Phys Chem B 107:1370
7. Roy B, Ahrenkiel SP, Fuierer PA (2008) J Am Ceram Soc 91:2455
8. Roy B, Fuierer PA (2010) J Am Ceram Soc 93:436
9. Cullity BD, Stock SR (1978) Elements of X-ray diffraction. Addison-Wesley, Reading
10. Tan B, Toman E, Li Y, Wu Y (2007) J Am Chem Soc 129:4162
11. Nakade S, Matsuda M, Kambe S, Saito Y, Kitamura T, Sakata T, Wada Y, Mori H, Yanagida S (2002) J Phys Chem B 106:10004
12. Sing KSW, Everett DH, Haul RAW, Moscou L, Pierotti RA, Rouquerol J, Siemieniewska T (1985) Pure Appl Chem 57:603
13. de Boer JH (1958) In: Everett DH, Stone FS (eds) The structure and properties of porous materials butterworth, London, UK
14. Kim J, Wilhelm O, Pratsinis SE (2001) J Am Chem Soc 84:2802
15. Song KC, Pratsinis SE (2001) J Am Chem Soc 84:92
16. Kumar KNP, Kumar J, Keizer K (1994) J Am Chem Soc 77:1396
17. Burnside S, Winkel S, Brooks K, Shklover V, Gratzel M, Hinsch A, Kinderman R, Bradbury C, Hagfeldt A, Pettersson H (2000) J Mater Sci 11:355. doi:10.1023/A:1008989601919
18. Yoshikawa Y, Tsuzuki YK (1992) J Am Chem Soc 75:2520
19. Swamy V, Kuznetsov A, Dubrovinsky LS, Caruso RA, Shchukin DG, Muddle BC (2005) Phys Rev B Condens Matter Mater Phys 71:184302
20. Diebold U, Hebenstreit W, Leonardelli G, Schmid M, Varga P (1998) Phys Rev Lett 81:405
21. Bohem HP (1966) Adv Catal 16:179
22. Craido J, Real C (1983) J Chem Soc Tran I 79:2765
23. Nakade S, Saito Y, Kubo W, Kitamura T, Wada Y, Yanagida S (2003) J Phys Chem B 107:8607
24. Hidalgo MC, Colón G, Nav′ıo JA (2002) J Photochem Photobiol A 148:341
25. Ohno T, Sarukawa K, Tokieda K, Matsumura M (2001) J Catal 203:82
26. Datye AK, Riegel G, Bolton JR, Huang M, Prairie MR (1995) J Solid State Chem 115:236
27. Kim H, Kushto GP, Arnold CB, Kafafi ZH, Piqué A (2004) Appl Phys Lett 85:464
28. Snaith HJ, Schmidt-Mende L, Grätzel M, Chiesa M (2006) Phys Rev B Condens Matter Mater Phys 74:045306
29. Green MA (1982) Solar cells operating principles, technology, and system applications. Prentice Hall, New Jersey